Supporting Information

Yao and Olvera de la Cruz 10.1073/pnas.1403679111

SI Text

Here we report the simulation results of using the alternative periodic boundary condition and present the additional information of multiple impurity particles. In addition, some technical details of the simulated annealing Monte Carlo (MC) simulations are given in the last section.

Periodic Boundary Condition

Simulations of confined soft particles using the hard wall boundary condition (HWBC) have shown that the presence of an impurity particle only influences the particles nearby. The regular crystalline lattice beyond a modest distance from the impurity particle is well protected by the proliferating topological defects. The HWBC is therefore justified. To further substantiate that the boundary effect is negligible, as numerically observed in confined systems, we perform simulations using the periodic boundary condition (PBC).

Fig. S1 demonstrates the periodic boundary condition used in simulations. All of the opposite edges of the hexagonal wall are identical as indicated by the arrows in Fig. S1. To physically glue together these opposite edges, we obtain the shape of a doughnut surface. In other words, a hexagonal domain with the specified periodic boundary condition is topologically equivalent to a torus. A particle on the upper edge (the upper green one in Fig. S1) can therefore interact with the particle near the opposite lower edge (the lower red one in Fig. S1).

Simulated annealing MC simulations using the PBC show that the particles near the boundary are immobile in comparison with the initial configuration where all of the particles are centered at the sites of a perfect hexagonal lattice (see the orderly arranged boundary particles in Fig. S2 for $N = 1,261$). They are literally not squeezed at all considering that the energy of the boundary particles (at the order of $10^{-39}\epsilon$, where ϵ is the energy scale in the expression for the Hertzian potential in the main text) is much smaller than that of the impurity particle (at the order of $10^{-2}\epsilon$ for $\Gamma \approx 2$). These observations are in perfect agreement with those in simulations based on the HWBC. Systematic simulations in systems whose size ranges from $N = 331$ to 2,791 further confirm that the feature of the intactness of boundary particles found in HWBC-based simulations is unaltered when switching to the PBC. Consequently, PBC-based simulations reproduce all of the key results in HWBC-based simulations. For example, the sixfold symmetric stress patterns are also found in PBC-based simulations with the increase of Γ, as shown in Fig. S2 *C* and *D*. The delay of the appearance of topological defects due to the softened potential is also observed in PBC-based simulations. In addition, the evolution of the defect motifs from neutral quadrupole to trapped disclination at the site of the impurity with the expansion of the impurity particle is recovered in PBC-based simulations. The basic screening scenario composed of bounding counter disclinations and scattered neutral defects around the impurity particle is also found in a wide range of the values for the parameter Γ. Specifically, the critical values $\Gamma_{\text{critical}} \approx 2.55$ for the appearance of the trapped central disclination is identical to the one obtained in HWBC-based simulations. Neutral quadrupoles start to appear at $\Gamma = 2.3$ in PBC-based simulations, in contrast with $\Gamma = 2.2$ in simulations using the HWBC; this slight deviation may be attributed to the fact that a quadrupole has little effect on the system energy, as has been discussed in the main text. Fig. S2 shows the topological defect motifs and the corresponding stress patterns at critical states of $\Gamma = 2.3$ and 2.55 according to the simulations using the PBC.

These simulation results based on the alternative PBC exclude the possible influence of boundary on the response of the system to impurity particles. Moreover, the local physical effect of impurity particles in hexagonal lattices is further confirmed in these independent simulations using different boundary conditions.

Multiple Impurity Particles

In the main text, we have discussed the interaction of two approaching impurity particles. In this section, we present more results for the case of multiple impurity particles.

Specifically we study cases where the impurity particles are symmetrically distributed as shown in Fig. S3 *A*–*C* for three impurity particles and Fig. S3 *D*–*F* for six impurity particles. As in systems containing two impurity particles, we also observe the reduction of the energy with the approach of the multiple impurities. Fig. S4 *A* and *B* shows the variation of the energy vs. the distance d from the impurity particles to the center of the disk for three and six impurities, respectively. The concurrence of the proliferation of induced defects and the reduction of the energy for $d < 8\sigma_0$ is also found in simulations of multiple impurities. The basic physics underlying the numerically observed short-range attraction of multiple impurity particles is the same as that in the case of two impurities; the proliferation of topological defects with the approach of impurities plays a crucial role.

The typical topological defect motifs as well as the stress distribution are given in Fig. S3 for three and six impurities. When the impurity particles are separated by as far as about $20\sigma_0$, they can be treated as independent entities without interactions as seen from the associated stress patterns in Fig. S3 *A* and *D*. The approach of these impurity particles toward the center of the system leads to the proliferation of defects; these induced defects initially appear near one or two impurity particles instead of surrounding all the impurity particles simultaneously. For the specific case of six impurity particles at $\Gamma = 2.0$, we find that the induced defects are distributed between the six "uncharged" impurity particles (Fig. S3 *E* and *F*).

Some Details of the Simulated Annealing MC Algorithm

In the cooling schedule of the simulated annealing MC algorithm, the initial temperature is set to be a fraction of the energy scale ϵ in the expression for $V(r)$. The temperature in the MC simulations is decreased at the typical rate of $dT/T \sim 10^{-6}$ once the reduction rate of the system energy becomes very slow, typically $dE/E \sim 10^{-7}$. In the search for the proper values for these parameters, the above choices can produce the lowest energy states among all of the trials. About 10^6 MC sweeps are carried out for each run; each MC sweep consists of trial attempts to randomly move each particle. The acceptance or rejection of a MC trial is determined by the standard Metropolis algorithm. The quality of simulations is controlled by tracking the energy variation in all of the MC steps. The simulations can distinguish states whose energy difference is within 0.1%, indicating that the numerical scheme we adopted can lead us deep to the energy basins. We introduce the Delaunay triangulation to analyze the finally obtained low-energy configurations.

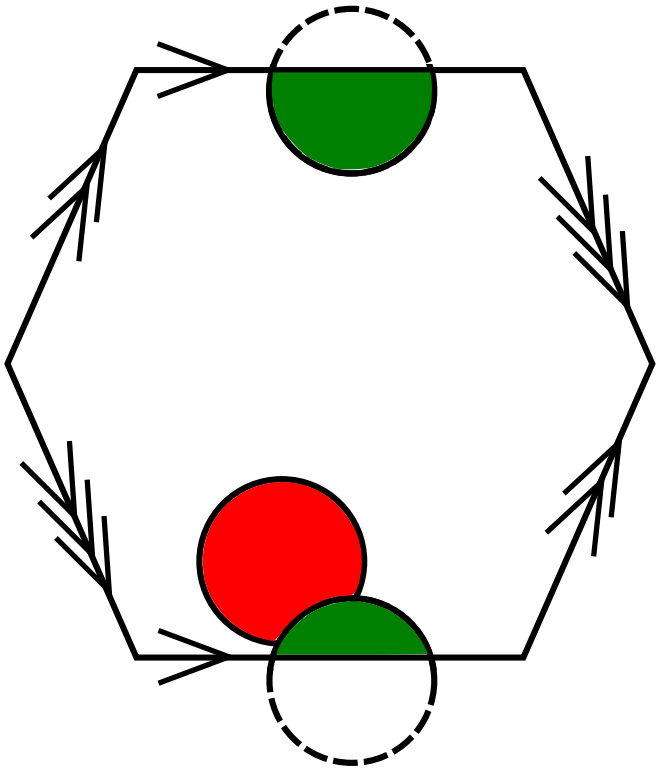

Fig. S1. Illustration of the PBC used in simulations. All of the opposite edges of the hexagonal wall are identical as indicated by the arrows. To physically glue together these opposite edges, we obtain the shape of a doughnut surface. The interaction between the upper green and the lower red particles is therefore possible.

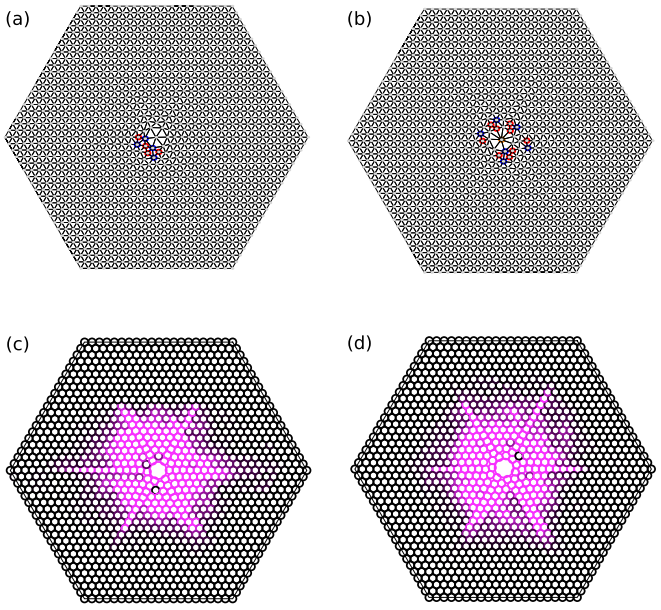

Fig. S2. Evolution of topological defects and the stress pattern with the expansion of the impurity particles according to the simulations using the PBC. (*A*) $\Gamma = 2.3$, (*B*) 2.55. (*C* and *D*) The corresponding stressed regions are shown. The number of particles is $N = 1{,}261$.

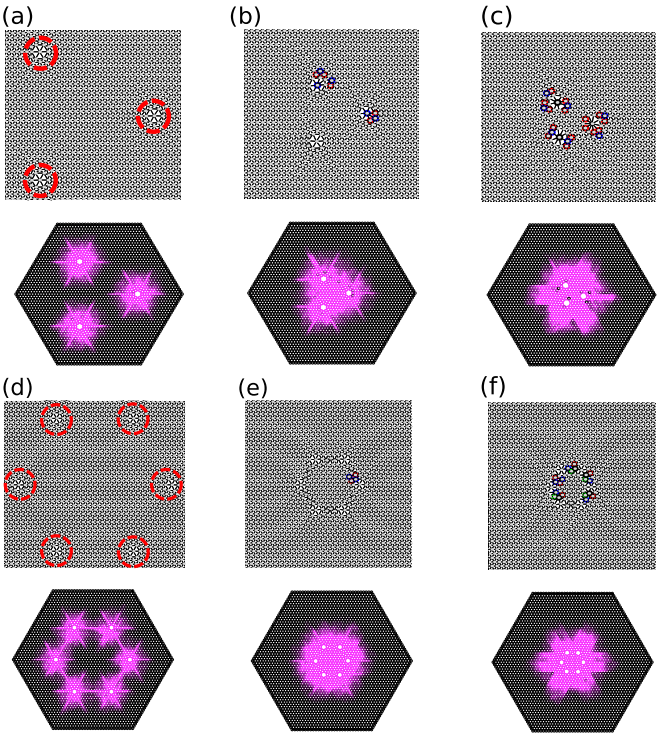

Fig. S3. Evolution of topological defects and the stress pattern with the approach of the impurity particles. The number of impurity particles is (*A*–*C*) 3 and (*D*–*F*) 6. The positions of impurities are indicated by red circles in the defect-free states or the white disks in the stress patterns. The distances from the impurity particles to the center of the disk are (*A* and *D*) $14\sigma_0$, (*B* and *E*) $6\sigma_0$, and (*C* and *F*) $4\sigma_0$, respectively. Disclinations of different types in *A*–*C* are distinguished by colors; fourfold disclinations in green, fivefold in red, sevenfold in blue, and eightfold in black. (*A*–*C*) $\Gamma = 2.5$ and (*D*–*F*) 2. The number of particles is $N = 2{,}791$.

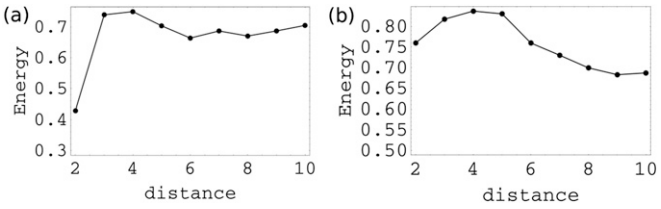

Fig. S4. Energy vs. distance from the impurity particles to the center of the disk. The number of impurity particles is (*A*) 3 and (*B*) 6. (*A*) $\Gamma = 2.5$ and (*B*) $\Gamma = 2$. The distance is measured in the unit of $2\sigma_0$. The number of particles is $N = 2{,}791$.